

$^{70}\text{Ge}(p,\gamma)^{71}\text{As}$ and $^{76}\text{Ge}(p,n)^{76}\text{As}$ cross sections for the astrophysical p process: sensitivity of the optical proton potential at low energies

G. G. Kiss,* Gy. Gyürky, Z. Elekes, Zs. Fülöp, and E. Somorjai
Institute of Nuclear Research (ATOMKI), H-4001 Debrecen, POB.51., Hungary

T. Rauscher
Universität Basel, CH-4056 Basel, Switzerland

M. Wiescher
University of Notre Dame, Notre Dame, Indiana 46556, USA
 (Dated: October 29, 2018)

The cross sections of the $^{70}\text{Ge}(p,\gamma)^{71}\text{As}$ and $^{76}\text{Ge}(p,n)^{76}\text{As}$ reactions have been measured with the activation method in the Gamow window for the astrophysical p process. The experiments were carried out at the Van de Graaff and cyclotron accelerators of ATOMKI. The cross sections have been derived by measuring the decay γ -radiation of the reaction products. The results are compared to the predictions of Hauser-Feshbach statistical model calculations using the code NON-SMOKER. Good agreement between theoretical and experimental S factors is found. Based on the new data, modifications of the optical potential used for low-energy protons are discussed.

PACS numbers: 25.40.Lw, 26.30.+k, 26.50.+x, 27.50.+e

I. INTRODUCTION

The stable proton-rich nuclei with charge number $Z \geq 34$ are called p nuclei [1]. The natural isotopic abundance of these nuclei is 10 – 100 times less than the more neutron-rich isotopes. Most p nuclei cannot be produced by neutron capture because they are separated by unstable short-lived nuclei from the s or r process path. It is generally accepted that the main stellar mechanism synthesizing these nuclei – the so-called p process – is initiated by (γ,n) photodisintegration reactions on pre-existing more neutron-rich seed nuclei. As the neutron separation energy increases along this path towards more neutron deficient isotopes, (γ,p) and (γ,α) reactions become stronger and process the material towards lower masses [2, 3, 4]. Despite considerable experimental and theoretical efforts in recent years, there are still open questions about the nature of the p process and the synthesis of the p isotopes.

The high intensity energetic photons necessary for these γ -induced reactions are available only in scenarios with temperatures around 2-3 GK. One possible site for such a scenario is the O-Ne layer of a massive star in hydrostatic pre-supernova burning or explosive burning due to the type II supernova shockwave. Other potential sites providing the necessary conditions for p process nucleosynthesis have been summarized recently [2]. One of the main uncertainties in p process nucleosynthesis is associated with the origin of the light Mo, Ru, In, and Sn p -nuclei with a fairly large abundance which cannot be explained in the framework of standard p process

nucleosynthesis models. It has been argued that the p process might be complemented by other nucleosynthesis processes such as the rp process for the light p nuclei ($A \leq 100$) [5] or the neutrino induced νp process in type II supernovae [6]. Additional possibilities are discussed in [2].

Modeling the synthesis of the p nuclei and calculating their abundances require an extended reaction network calculation involving more than 10000 reactions on 2000 stable and unstable nuclei. Most of the reaction rates are calculated by using the Hauser-Feshbach statistical model. The rates of the γ -induced reactions can be determined experimentally by measuring the inverse reaction cross section and converting the results by using the detailed balance theorem. In contrast to neutron-capture reactions which are comparatively well studied over the relevant mass region of the stable isotopes, charged particle induced reactions at energies below the Coulomb barrier are only scarcely studied for the mass region above iron. Previous [1] and recent [3, 4] investigations agree on the fact that (γ,α) reactions are mainly important at higher masses while (γ,p) reactions are more important for the lighter p nuclei. In recent years a range of (α,γ) reaction cross sections on ^{70}Ge , ^{96}Ru , ^{106}Cd , ^{112}Sn , and ^{144}Sm have been measured, and the results have been compared with model predictions [7, 8, 9, 10, 11]. In general the models were able to reproduce the experimental data within a factor of two; in some cases, however, larger deviations have been observed.

Beside these studies, numerous (p,γ) experiments have been performed on stable p nuclei to determine the reaction rates of the corresponding (γ,p) reactions [12, 13, 14, 15, 16, 17, 18, 19, 20, 21, 22]. These proton capture studies have shown better agreement between experimental results and theoretical predictions than in the case of alpha capture reactions discussed above. However, the ex-

*Electronic address: ggkiss@atomki.hu

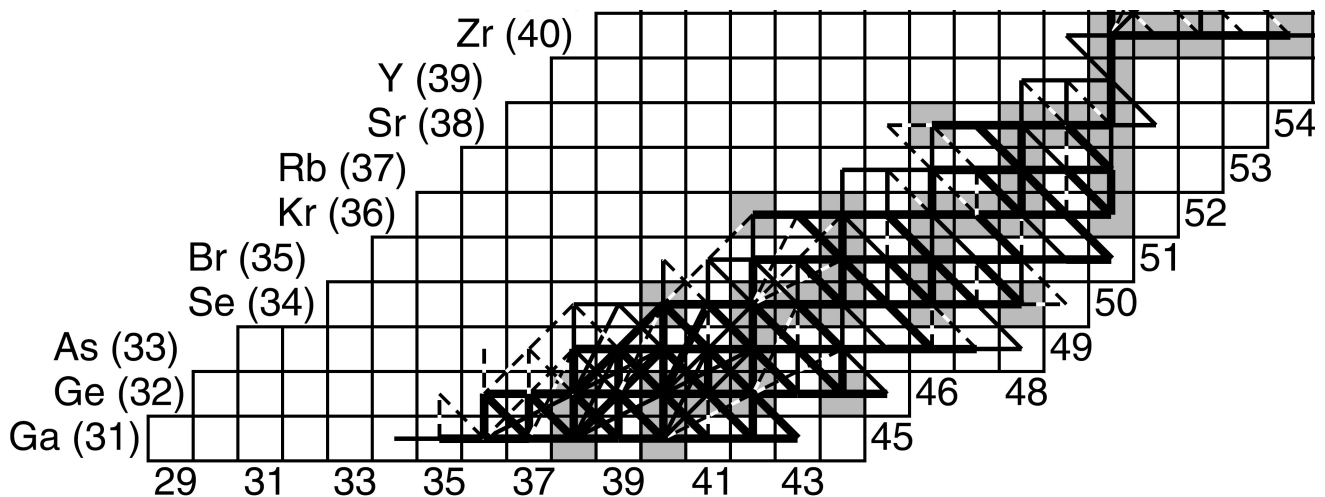


FIG. 1: Integrated reaction flux of the p process in the Ga to Zr mass range during the first second of a type II SN explosion triggering a shock front in the Ne/O layer with a maximum temperature of $T = 3$ GK. The strength of reaction flux is indicated by line thickness. Figure is taken from [4].

isting experimental database is not sufficient for a global check of the reliability of model calculations; further experimental data are clearly needed [3, 4].

As will be further elaborated in the discussion section of this paper, (p,n) reactions generally are better suited to study the impact of the optical potential used for protons. While uncertainties in both the proton and γ widths impact the cross section prediction in the experimentally accessible energy range of capture reactions, the theoretical uncertainties in (p,n) reactions are dominated by the proton width alone. Thus, (p,n) studies allow global testing of the proton potential whereas (p, γ) ones directly study astrophysically important reactions.

Moreover, it was demonstrated recently that (p,n) reactions on s or r process seed nuclei do affect the abundances of the light p nuclei [4]. There is only limited experimental information available about the low energy cross sections of critical (p,n) reactions in this mass range. This is demonstrated in the case of $^{75}\text{As}(p,n)^{75}\text{Se}$, where the existing data [23, 24] show considerable discrepancies which makes a direct comparison with Hauser Feshbach predictions difficult [4]. A reliable simulation of the rather complex p process nucleosynthesis pattern in this mass range is of great relevance in particular to differentiate between the contributions from p process, s process, and r process sites. This also requires testing the applicability and reliability of the global Hauser Feshbach predictions in this mass range.

In this paper we want to pursue our studies investigating the cross sections of $^{70}\text{Ge}(p,\gamma)^{71}\text{As}$ and $^{76}\text{Ge}(p,n)^{76}\text{As}$ which are both associated with the reaction flow pattern in this mass range as demonstrated by [4]. Figure 1 shows the complex reaction pattern during the first second of the shock front induced p process. The reaction $^{70}\text{Ge}(p,\gamma)^{71}\text{As}$ corresponds to a branch associated with the final abundance of the p nucleus ^{70}Ge in the p process. The proton capture di-

TABLE I: Decay parameters of $^{70}\text{Ge}(p,\gamma)^{71}\text{As}$ and $^{76}\text{Ge}(p,n)^{76}\text{As}$ reaction products taken from the literature.

Product nucleus	Half-life [hour]	Gamma energy [keV]	Relative γ -intensity per decay [%]	Ref.
^{71}As	65.28 ± 0.15	174.95 ± 0.04	82.00 ± 0.25	[25]
		326.79 ± 0.02	3.03 ± 0.03	
		499.91 ± 0.01	3.62 ± 0.02	
		1095.51 ± 0.01	4.08 ± 0.06	
^{76}As	25.87 ± 0.05	559.10 ± 0.01	44 ± 1	[26]
		657.04 ± 0.01	6.2 ± 0.3	

rection gives rise to depletion of this nucleus at low p process temperatures whereas the reverse rate can produce it through a (γ,n) - (γ,p) branching at higher temperature. The reaction $^{76}\text{Ge}(p,n)^{76}\text{As}$ is directly associated with the transformation of the r process seed nucleus ^{76}Ge to the p nucleus ^{74}Se in the first moments of p process nucleosynthesis; for example through the $^{76}\text{Ge}(p,n)^{76}\text{As}(\gamma,n)^{75}\text{As}(p,n)^{75}\text{Se}(\gamma,n)^{74}\text{Se}$ reaction chain. Fig. 1 suggests that many alternative reaction sequences exist, but it also underlines that during the p process ^{76}Ge is not only depleted but also produced by an initial $^{74}\text{Ge}(n,\gamma)^{75}\text{Ge}(n,\gamma)^{76}\text{Ge}$ reaction flux. This modifies the initial ^{76}Ge abundance. A detailed knowledge of the reaction rate of $^{76}\text{Ge}(p,n)^{76}\text{As}$ as the sole depletion process is important to investigate the overall nucleosynthesis pattern and history of ^{76}Ge in a type II supernova shock front environment.

In the following we outline the experimental approach

for measuring $^{70}\text{Ge}(p,\gamma)^{71}\text{As}$ and $^{76}\text{Ge}(p,n)^{76}\text{As}$ using the activation method. We describe the experimental set-up and procedure and finally present the experimental results. A concluding discussion section contains a detailed theoretical analysis of the results and their importance for the prediction of low-energy optical potentials.

II. INVESTIGATED REACTIONS

To determine the cross sections we used the activation method. This method allows to measure several cross sections simultaneously using natural targets. The element Ge has five stable isotopes with mass numbers $A=70, 72, 73, 74,$ and 76 , having isotopic abundances of 20.37%, 27.31%, 7.76%, 36.73%, and 7.83%, respectively [27]. The number of reaction channels measurable with the activation method is limited. Specifically, because of the low (p,n) thresholds the $^{73,74}\text{Ge}(p,n)$ reactions cannot be separated from the $^{72,73}\text{Ge}(p,\gamma)$ ones. It is also impossible to measure the cross sections of the $^{74}\text{Ge}(p,\gamma)^{75}\text{As}$ and $^{76}\text{Ge}(p,\gamma)^{77}\text{As}$ reactions because ^{75}As is stable and in the case of the second reaction the γ -intensity from the decay of the final nucleus is very weak. The $^{70,72}\text{Ge}(p,n)$ reaction channels are not open in the investigated energy region.

In summary, it proved feasible to measure the proton induced cross sections of the reactions $^{70}\text{Ge}(p,\gamma)^{71}\text{As}$ and $^{76}\text{Ge}(p,n)^{76}\text{As}$ in the energy range $E_{c.m.} = 1.6-4.3$ MeV. This energy range covers the Gamow window for typical p process temperatures. The decay parameters used for the analysis are summarized in Table I.

III. EXPERIMENTAL PROCEDURE

A. Target properties

The targets were made by evaporating natural metallic Ge on thin, high purity Al foils. Aluminum backings were used because Al has only one stable isotope. The reaction product of $^{27}\text{Al}(p,\gamma)^{28}\text{Si}$ is stable and the (p,n) channel opens only at $E_{c.m.} = 5.59$ MeV which is above our investigated energy range. Moreover, Al can be easily distinguished from Ge in the Rutherford Backscattering (RBS) spectrum that was used to monitor the target stability, see below. These reasons make Al ideal as backing material in low-energy proton-induced reactions using the activation technique. The thickness of the targets has been derived by weighing. The weight of the Al backing was measured before and after the Ge evaporation. We repeated the mass measurement of the target also after the irradiation to prove that no changes in the number of the target atoms occurred during the irradiation.

The thickness of the targets varied between 50 and 290 $\mu\text{g}/\text{cm}^2$, corresponding to a proton energy loss of ≈ 2 keV ($E_p = 4.4$ MeV) and ≈ 25 keV ($E_p = 1.6$ MeV),

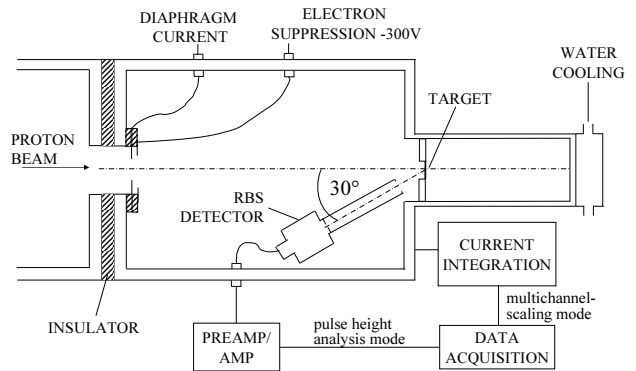


FIG. 2: Schematic view of the target chamber used for the irradiations

respectively. The proton energy loss was calculated using the SRIM [28] code. Thicker targets were used at low bombarding energy, where the cross section and the corresponding γ -yield is small. Even in the case of the thickest target at the lowest proton energy, the energy loss was ≈ 25 keV which is small compared to the 400 keV energy steps (see below).

B. Irradiation and activity determination

The irradiations were carried out at the Van de Graaff and cyclotron accelerators of ATOMKI. The energy range ($E_p = 1.6$ to 4.4 MeV) was covered with 400 keV steps. A schematic view of the target chamber is shown in Fig. 2. Downstream the diaphragm the whole chamber served as a Faraday cup. The collected charge was measured with a current integrator. At the entrance of the chamber another diaphragm was used with -300 V secondary electron suppression voltage.

Each irradiation lasted between 3 and 11 h. Before the experiment several beam tests were performed to verify target stability. These tests showed that there was no deterioration of the targets using a proton beam current less than 500 nA. A surface barrier detector was built into the chamber at $\Theta=150^\circ$ relative to the beam direction. This detector was used to monitor the target stability during the irradiation. The RBS spectra were taken continuously and stored regularly during the irradiation.

The collected charge varied between $\approx 5-20 \times 10^{-3}$ C in the case of each irradiation. The current integrator counts were recorded in multichannel scaling mode, stepping the channel in every 10 s to take into account the possible changes in the beam current.

Between the irradiation and the γ counting, a waiting time of 0.5 h was inserted in order to decrease the yield of the disturbing short-lived activities. The γ radiation following the β decay of the produced As isotopes was measured with a 40% relative efficiency HPGe detector.

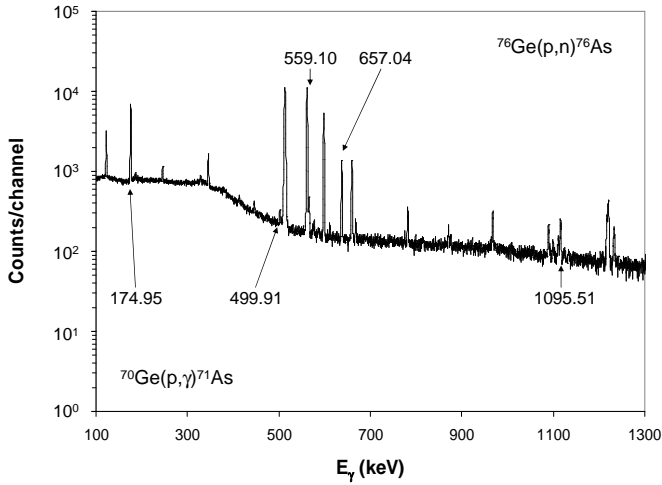


FIG. 3: Off-line γ spectrum taken after the irradiation using 3.2 MeV proton beam. The marked γ peaks were used for the analysis. The other peaks correspond to laboratory background or beam induced background on impurities in the target or the backing.

A 10 cm thick lead shield was used to reduce the laboratory background. The γ spectra were taken for 10 h and stored regularly in order to follow the decay of the different reaction products.

The absolute efficiency curve of the detector was measured using calibrated ^{137}Cs , ^{60}Co , and ^{152}Eu sources in the same geometry. The measured points were fitted with a third-degree logarithmic polynomial to determine the efficiency curve for the energy region of interest. The efficiency of the detector was also studied with Monte Carlo simulations using the GEANT code [29]. Good agreement was found between the efficiency curve calculated with GEANT and the polynomial fit. As an example, Fig. 3 shows a collected off-line γ spectrum after irradiation using a 3.2 MeV proton beam.

IV. EXPERIMENTAL RESULTS

Table II summarizes the experimental cross sections and S factors for the two investigated reactions. Figure 4 shows the results in comparison to the Hauser-Feshbach statistical model prediction, using the NON-SMOKER code [32] with standard settings as given in [30, 31]. The uncertainties of the center-of-mass energies given in the second column of Table II correspond to the energy loss in the target calculated with the SRIM code and for the energy stability of the beam. The uncertainty in the cross section (S factor) values is the quadratic sum of the following partial uncertainties: efficiency of the HPGe detector ($\approx 7\%$), number of target atoms ($\approx 6\%$), current measurement ($\approx 3\%$), uncertainties of the level parameters found in literature [25, 26] ($\leq 1\%$), and counting statistics (0.8 to 11%).

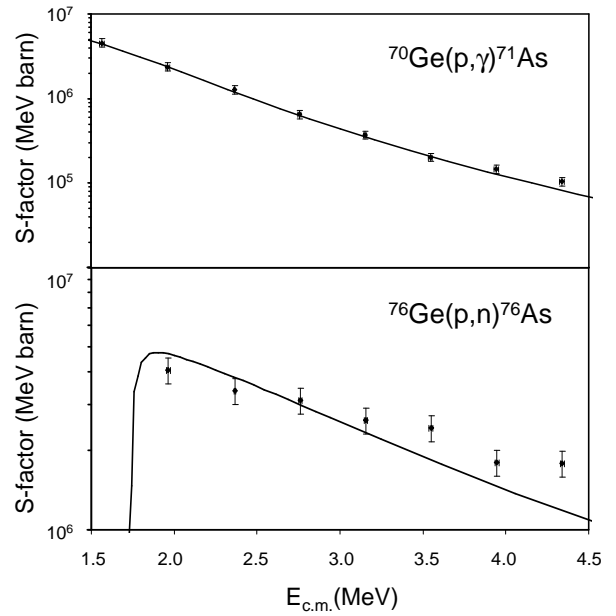


FIG. 4: Measured S factor of the $^{70}\text{Ge}(p,\gamma)^{71}\text{As}$ and $^{76}\text{Ge}(p,n)^{76}\text{As}$ reactions compared to previous NON-SMOKER results [30, 31].

TABLE II: Experimental cross sections and S factors of the $^{70}\text{Ge}(p,\gamma)^{71}\text{As}$ and $^{76}\text{Ge}(p,n)^{76}\text{As}$ reactions.

E_{beam} [keV]	$E_{\text{c.m.}}^{\text{eff}}$ [keV]	Cross section [mb]	S factor [10^6 MeV b]
$^{70}\text{Ge}(p,\gamma)^{71}\text{As}$			
1600	1565 ± 13	0.035 ± 0.004	4.5 ± 0.5
2000	1963 ± 13	0.22 ± 0.03	2.4 ± 0.3
2400	2363 ± 4	0.71 ± 0.08	1.3 ± 0.1
2800	2757 ± 9	1.4 ± 0.2	0.65 ± 0.07
3200	3152 ± 10	2.4 ± 0.3	0.37 ± 0.04
3600	3545 ± 12	3.2 ± 0.4	0.20 ± 0.02
4000	3942 ± 12	4.9 ± 0.6	0.15 ± 0.02
4400	4336 ± 13	6.8 ± 0.8	0.11 ± 0.01
$^{76}\text{Ge}(p,n)^{76}\text{As}$			
2000	1965 ± 13	0.37 ± 0.04	4.0 ± 0.4
2400	2366 ± 4	1.9 ± 0.2	3.4 ± 0.4
2800	2760 ± 9	6.8 ± 0.8	3.1 ± 0.3
3200	3156 ± 10	17 ± 2	2.6 ± 0.3
3600	3549 ± 12	40 ± 4	2.4 ± 0.3
4000	3946 ± 12	62 ± 7	1.8 ± 0.2
4400	4341 ± 13	115 ± 13	1.8 ± 0.2

V. DISCUSSION

A. Comparison to theory

The proton capture data is excellently predicted by the previously published NON-SMOKER Hauser-Feshbach calculation [30, 31]. Also the (p,n) data is reproduced reasonably well although the data seem to indicate a slightly different slope of the S factor as function of energy. Since the computation of the relevant quantity for astrophysics, the reaction rate, involves an integration across the energy range given by the Gamow peak (see, e.g., [33]), the observed deviation is averaged out and barely appears in the rates at p -process temperatures. Nevertheless, it is worthwhile to study the origin of the different behavior of the relation between data and predictions in the two cases of radiative capture and (p,n) reaction.

At first, it has to be realized that the theoretical (p, γ) and (p,n) results exhibit different dependences on nuclear inputs. The averaged statistical model cross sections $\langle \sigma \rangle_{\text{HF}}$ are derived from averaged widths $\langle \Gamma \rangle$, leading to an expression similar to that of resonant reactions [34]

$$\langle \sigma \rangle_{\text{HF}} \propto \frac{\langle \Gamma \rangle_i \langle \Gamma \rangle_o}{\langle \Gamma \rangle_{\text{tot}}} \quad , \quad (1)$$

with i , o labeling the entrance and exit channel, respectively, and $\langle \Gamma \rangle_{\text{tot}}$ being the averaged total width including all possible deexcitation channels (particle and photon emission) of the compound nucleus. As is well-known in the resonant case, the energy dependence is then determined by the smallest width in the numerator of Eq. (1). The situation is more involved if the widths are of similar magnitude or if another channel is significantly contributing to the total width.

In order to study the sensitivities of the calculated S factors, we systematically and independently varied the averaged widths of the neutron, proton, and γ channels by factors of 2 up and down. As expected, the (p,n) S factor is only sensitive to variations in the proton width $\langle \Gamma \rangle_p$ in the entrance channel, except for an energy range of up to about 100 keV above the threshold where neutron widths are still small. This shows that the (p,n) reaction is well suited to study the impact of the optical potential used to compute the proton widths.

The situation is more complicated in the (p, γ) case. All widths were varied but only the proton and γ widths were found to be important. The sensitivity to a variation of the proton and γ widths is shown in Fig. 5, with the sensitivity s assuming values between Zero and One. It is defined via the variation of the cross section (S factor) $\Delta\sigma = s\delta$, with the width variation factor δ chosen to be 2 and 0.5, respectively. As can be seen in Fig. 5 the S factor is mostly sensitive to the proton widths at energies below about 2.5 MeV. Above that energy the γ width sensitivity becomes comparable or larger. This

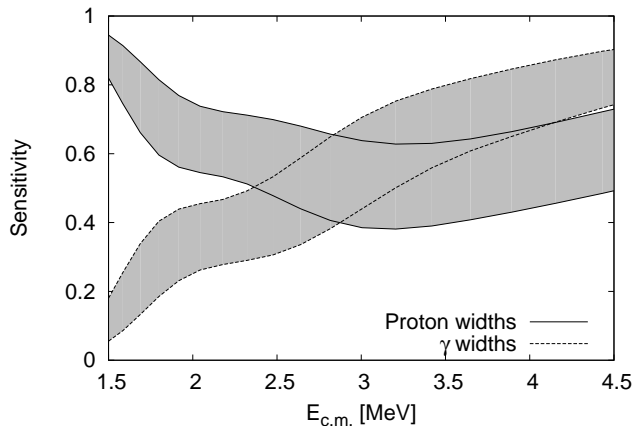


FIG. 5: Sensitivity of the theoretical $^{70}\text{Ge}(p,\gamma)^{71}\text{As}$ results to variations of the widths as function of proton energy. The area between the solid lines shows the sensitivity to variations of the proton widths, the one between the dashed lines is the sensitivity to varied γ widths.

implies that – contrary to the (p,n) reaction which is sensitive to the proton width at all measured energies – the S factor is mostly sensitive to the proton width at the lowest energy. The excellent agreement of theory and measurement shows that the proton width is described well at low energies and that γ widths are described well at the upper end of the measured energy range.

For completeness, also the impact of a variation of the nuclear level density was studied. The nuclear level densities in the target and final nucleus determine the number of possible transitions in the entrance and exit channel, respectively, and thus impact the size of averaged widths. In the cases studied here, however, a variation of the nuclear level density does not have any impact. This is because the calculation uses up to 20 discrete experimental levels in each nucleus at low excitation energies (see Ref. [31] for a list of the levels). In all cases studied here, transitions to those lowest levels dominate the widths and therefore varying the nuclear level density employed above these levels does not change the result.

B. Modification of the optical potential

Apparently, the optical potential used for calculation of the proton widths gives rise to the different energy dependence of the theoretical (p,n) S factor as compared to experiment. The optical potential used here is the widely-used semi-microscopic potential of [35] with low-energy modifications by [36] (this will be addressed as JLM potential in the following), based on an infinite nuclear matter calculation employing the Reid hard core interaction, the Brückner-Hartree-Fock approximation, and a local density approximation. It has been argued [37] that the JLM potential may have to be improved above 160 MeV projectile energy and that its isovector

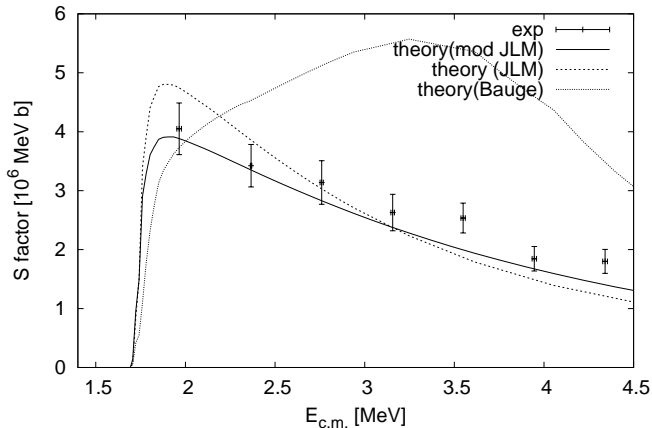


FIG. 6: Astrophysical S factor as function of proton energy for the reaction $^{76}\text{Ge}(p,n)^{76}\text{As}$. Experimental S factors measured in this work are compared to NON-SMOKER calculations using the optical potentials of [35, 36] (JLM), of [38] (Bauge), and a modified JLM potential with an increased imaginary strength (see text).

components may be too weak. The former is not relevant here but the latter can also have an impact at the low energies of astrophysical interest. A new parameterization of the JLM model has been derived in [37] and then improved to be Lane-consistent, i.e. equally applicable to neutrons and protons, in [38]. A comparison of our (p,n) data with the results obtained when using this latter potential is shown in Fig. 6. Obviously, the original JLM potential still fares much better in reproducing both the energy dependence and the absolute magnitude of the S factor. Similar problems were already found for Se isotopes in [20]. Fig. 7 shows that the low-energy S factor of the (p, γ) reaction is severely underpredicted. The agreement at the upper end of the measured energy range is not surprising because the sensitivity to the proton potential is smaller there, as discussed above.

We have attempted to improve the JLM potential by modifying the strengths of its real and imaginary parts. We find that an increase of the imaginary strength by 70% yields the best compromise in reproducing both the (p,n) and (p, γ) data, as shown in Figs. 6 and 7. The results are extremely sensitive to a variation of the real part and therefore best agreement is found when adopting the original real strength. A behavior similar to the results when using the potential of [38] is found for the (p, γ) reaction when increasing the real part only slightly.

Since both the isoscalar and isovector parts of the JLM model contribute to the imaginary part, we cannot disentangle their individual importance. Following the argumentation of [37], we attribute the increase in the imaginary part to a stronger isovector component. However, the isovector component of the real part has to remain unchanged. It is conceivable that a different low-energy parameterization of the JLM model may yield similar results.

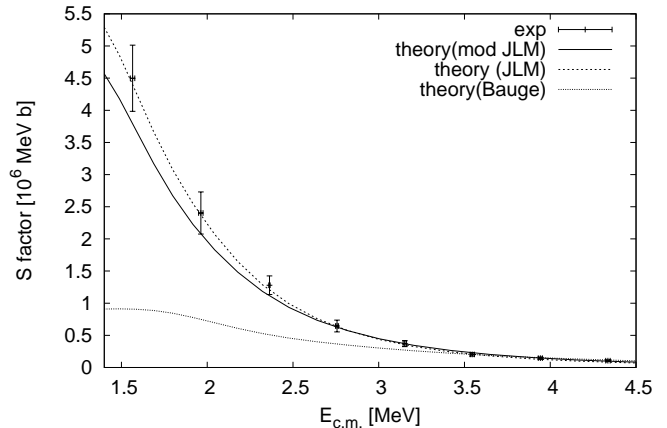


FIG. 7: Astrophysical S factor as function of proton energy for the reaction $^{70}\text{Ge}(p,\gamma)^{71}\text{As}$. Experimental S factors measured in this work are compared to NON-SMOKER calculations using the optical potentials of [35, 36] (JLM), of [38] (Bauge), and a modified JLM potential with an increased imaginary strength (see text).

Radiative proton capture and (p,n) reactions at astrophysically relevant energies in this mass region were previously studied involving Sr [16] and Se isotopes [20]. It is interesting to note that our modified JLM potential also leads to an improved prediction of the reactions $^{84,86,87}\text{Sr}(p,\gamma)^{85,87,88}\text{Y}$, $^{74,76}\text{Se}(p,\gamma)^{75,77}\text{Br}$, and $^{82}\text{Se}(p,n)^{82}\text{Br}$, as shown in Figs. 8–13 (compare with NON-SMOKER standard results given in the original plots of [16, 20]). Now all S factors are well reproduced, except for the one of $^{87}\text{Sr}(p,\gamma)^{88}\text{Y}$. Although the theoretical S factors have come closer to the experimental ones, there still remains a discrepancy of about a factor of Two. We were not able to establish an unambiguous explanation for this discrepancy. The predicted cross sections are insensitive to the theoretical nuclear level density employed, the level schemes of ^{87}Sr and ^{88}Y are sufficiently well established at low excitation energies, and the deformations of the nuclei involved are comparable to those of the other cases studied. The only difference from the experimental point of view is the much longer half-life of ^{88}Y (106.7 d). This is longer by a factor of at least 200 than the half-lives of the other final nuclei appearing in the activation experiments.

It should be mentioned that the JLM approach is also used for neutron potentials. However, whether the modified imaginary strength also applies to those cannot be determined within the framework of this paper.

C. Astrophysical reaction rates

The quantity of primary interest for astrophysical calculations is the astrophysical reaction rate. The relevant plasma temperature range for classical p process studies is 2 – 3 GK [2, 3]. We derived the reaction rates for the

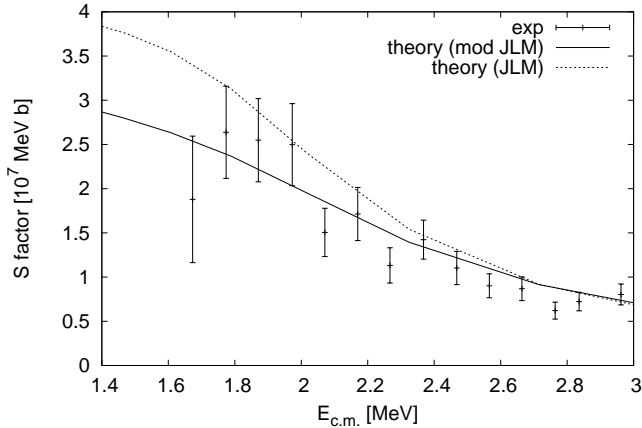


FIG. 8: Astrophysical S factor as function of proton energy for the reaction $^{84}\text{Sr}(p,\gamma)^{85}\text{Y}$. Experimental S factors from [16] are compared to NON-SMOKER calculations using the JLM potential (dashed line) and a modified JLM proton potential (solid line) with an increased imaginary strength (see text).

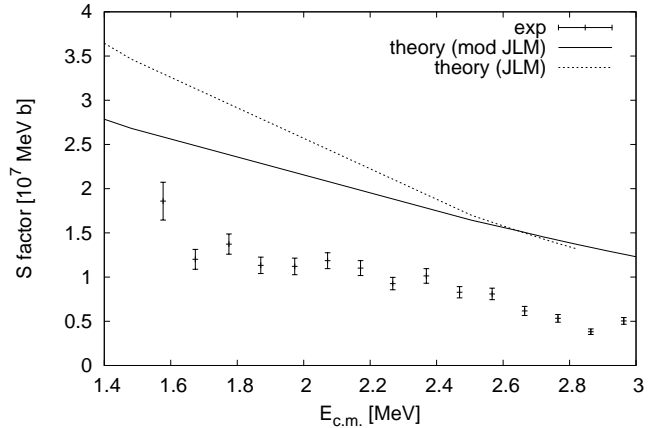


FIG. 10: Astrophysical S factor as function of proton energy for the reaction $^{87}\text{Sr}(p,\gamma)^{88}\text{Y}$. Experimental S factors from [16] are compared to NON-SMOKER calculations using the JLM potential (dashed line) a modified JLM proton potential (solid line) with an increased imaginary strength (see text).

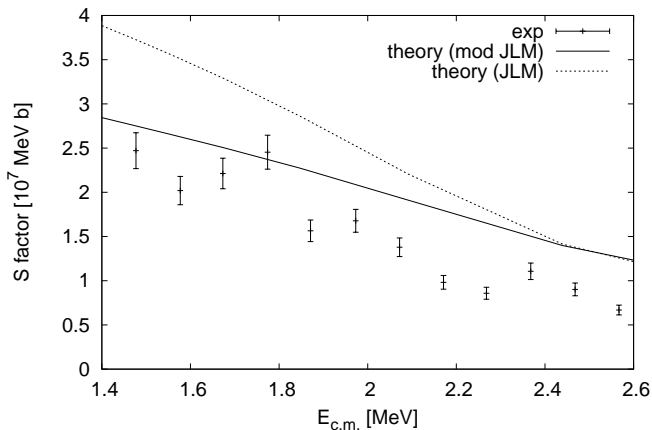


FIG. 9: Astrophysical S factor as function of proton energy for the reaction $^{86}\text{Sr}(p,\gamma)^{87}\text{Y}$. Experimental S factors from [16] are compared to NON-SMOKER calculations using the JLM potential (dashed line) a modified JLM proton potential (solid line) with an increased imaginary strength (see text).

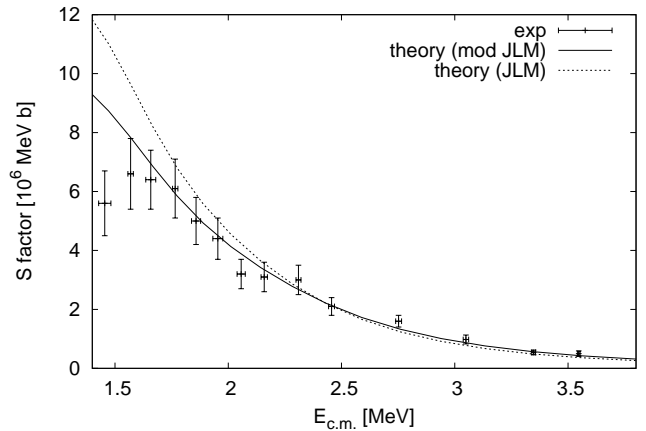


FIG. 11: Astrophysical S factor as function of proton energy for the reaction $^{74}\text{Se}(p,\gamma)^{75}\text{Br}$. Experimental S factors from [20] are compared to NON-SMOKER calculations using the JLM potential (dashed line) a modified JLM proton potential (solid line) with an increased imaginary strength (see text).

reactions measured in this work directly from the experimental S factors by linear interpolation and accounting for the error bars using the code EXP2RATE [39]. The numerical integration error is smaller than the experimental uncertainties.

Our data allow a computation of the rates for the temperature interval $(2.5 - 5.0) \times 10^9$ K in the case of $^{70}\text{Ge}(p,\gamma)^{71}\text{As}$. These rates are given in Table III. Obviously, these are ground state rates because they are derived from experimental data. However, there is no stellar enhancement due to thermal excitation of target states for this reaction in a stellar plasma (see, e.g., [30]) and therefore stellar and ground state rates are the same.

Because the data excellently confirm the prediction, the use of the tabulated rates in [30, 31] is recommended.

Due to the (p,n) threshold at 1.7 MeV, the reaction rate of $^{76}\text{Ge}(p,n)^{76}\text{As}$ can be calculated down to Zero temperature. To get a better description of the threshold behavior of the S factor, the theoretical values obtained with the modified JLM potential were used in the rate calculation below 1.565 MeV proton energy. The resulting rates are listed in Table IV. As in the previous reaction, these are ground state rates. The stellar enhancement predicted [30] for this reaction varies smoothly between 4% ($T_9 \leq 0.5$ and $3.0 \leq T_9 \leq 4.0$) and 10% (at $T_9 = 1.5$). Therefore it is negligible compared to the uncertainties in the rates stemming from the exper-

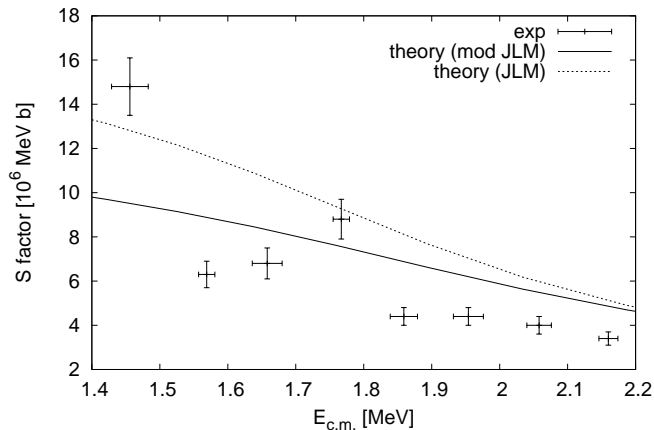


FIG. 12: Astrophysical S factor as function of proton energy for the reaction $^{76}\text{Se}(p,\gamma)^{77}\text{Br}$. Experimental S factors from [20] are compared to NON-SMOKER calculations using the JLM potential (dashed line) a modified JLM proton potential (solid line) with an increased imaginary strength (see text).

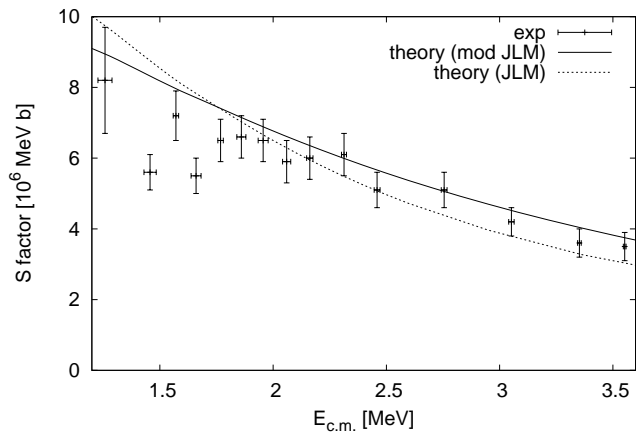


FIG. 13: Astrophysical S factor as function of proton energy for the reaction $^{82}\text{Se}(p,n)^{82}\text{Br}$. Experimental S factors from [20] are compared to NON-SMOKER calculations using the JLM potential (dashed line) a modified JLM proton potential (solid line) with an increased imaginary strength (see text).

imental uncertainties. In consequence, the rates quoted in Table IV can be taken as both ground state and stellar rates. Although the rates given in [30, 31] were obtained with the standard JLM potential and the S factors exhibit a slightly different slope, the new rates still agree reasonably well within errors with the predicted ones in the temperature range up to 4 GK.

It is worth to note that the reaction rate of the presently investigated two reactions has been measured by Roughton *et al.* [40]. On average the reaction rates obtained for the $^{70}\text{Ge}(p,\gamma)^{71}\text{As}$ reaction are 35% lower than the presently measured values and 20% higher for $^{76}\text{Ge}(p,n)^{76}\text{As}$ (the latter difference being within the error). The reaction rates in [40], however, have been de-

TABLE III: Astrophysical reaction rates of the reaction $^{70}\text{Ge}(p,\gamma)^{71}\text{As}$ computed from the experimental data. These are also stellar rates because the stellar enhancement is negligible.

Temperature [10^9 K]	Reaction Rate [$\text{cm}^3\text{s}^{-1}\text{mole}^{-1}$]
2.50	$(4.474 \pm 0.584) \times 10^2$
2.75	$(9.660 \pm 1.282) \times 10^2$
3.00	$(1.862 \pm 0.250) \times 10^3$
3.25	$(3.284 \pm 0.445) \times 10^3$
3.50	$(5.393 \pm 0.737) \times 10^3$
3.75	$(8.357 \pm 1.148) \times 10^3$
4.00	$(1.234 \pm 0.170) \times 10^4$
4.25	$(1.749 \pm 0.242) \times 10^4$
4.50	$(2.394 \pm 0.333) \times 10^4$
4.75	$(3.180 \pm 0.444) \times 10^4$
5.00	$(4.116 \pm 0.576) \times 10^4$

termined from thick target yields and no cross sections have been measured.

VI. SUMMARY

We have measured the cross sections of the reactions $^{70}\text{Ge}(p,\gamma)^{71}\text{As}$ and $^{76}\text{Ge}(p,n)^{76}\text{As}$ by the activation method and derived the astrophysical S factors in the c.m. energy range of 1.565 – 4.341 MeV. A comparison to predictions from the statistical model showed excellent agreement with the radiative proton capture data and good agreement with the (p,n) data although the energy dependence was not accurately reproduced for the latter. A detailed theoretical study led to the conclusion that the optical potential for protons can be modified in such a way as to reproduce both the (p, γ) and (p,n) data. It proved necessary to increase the depth of the imaginary part of the potential by a factor of 1.7. Also previously published data for low-energy (p, γ) and (p,n) reactions on Se and Sr isotopes can be reproduced well using this modified optical potential. It remains to be studied whether the modification is also applicable to other mass ranges, whether it should be energy dependent, and whether it should also be applied to neutron potentials. More data across a wider range of energies and masses would be needed for this.

The astrophysical reaction rates derived from the new data for $^{70}\text{Ge}(p,\gamma)$ and $^{76}\text{Ge}(p,n)$ are in agreement within the measured temperature range with the previously published ones [30, 31] which were based on Hauser-Feshbach calculations with the unmodified JLM potential.

Acknowledgments

This work was supported by OTKA (K68801, T49245, D48283), MTA-OTKA-NSF grant 93/049901, the Swiss

TABLE IV: Astrophysical reaction rates of the reaction ${}^{76}\text{Ge}(p,n){}^{76}\text{As}$ computed from the experimental data. These are also stellar rates because the stellar enhancement is negligible within the given uncertainty.

Temperature [10^9 K]	Reaction Rate [$\text{cm}^3\text{s}^{-1}\text{mole}^{-1}$]
0.25	0.000
0.50	$(3.086\pm 0.012)\times 10^{-12}$
0.75	$(2.118\pm 0.040)\times 10^{-6}$
1.00	$(1.912\pm 0.071)\times 10^{-3}$
1.25	$(1.222\pm 0.066)\times 10^{-1}$
1.50	$(2.088\pm 0.142)\times 10^0$
1.75	$(1.683\pm 0.133)\times 10^1$
2.00	$(8.487\pm 0.746)\times 10^1$
2.25	$(3.128\pm 0.296)\times 10^2$
2.50	$(9.231\pm 0.919)\times 10^2$
2.75	$(2.310\pm 0.239)\times 10^3$
3.00	$(5.091\pm 0.542)\times 10^3$
3.25	$(1.013\pm 0.110)\times 10^4$
3.50	$(1.856\pm 0.205)\times 10^4$
3.75	$(3.173\pm 0.355)\times 10^4$
4.00	$(5.114\pm 0.580)\times 10^4$

National Science Foundation (grants 200020-061031, 200020-105328) and the Joint Institute of Nuclear Astrophysics (www.JINAweb.org) NSF-PFC grant PHY02-16783. Gy. Gy. acknowledges financial support from the Bolyai grant.

- [1] S. E. Woosley and W. M. Howard, *Astrophys. J. Suppl.* **36**, 285 (1978).
- [2] M. Arnould and S. Goriely, *Phys. Rep.* **384**, 1 (2003).
- [3] T. Rauscher, *Phys. Rev. C* **73**, 015804 (2006).
- [4] W. Rapp, J. Görres, M. Wiescher, H. Schatz, and F. Käppeler, *Astrophys. J.* **653**, 474 (2006).
- [5] H. Schatz, A. Aprahamian, J. Görres, M. Wiescher, T. Rauscher, J. F. Rembes, F. -K. Thielemann, B. Pfeiffer, P. Möller, and K. -L. Kratz, *Phys. Rep.* **294**, 167 (1998).
- [6] C. Fröhlich, G. Martínez-Pinedo, M. Liebendörfer, F.-K. Thielemann, E. Bravo, W. R. Hix, K. Langanke, and N. T. Zinner, *Phys. Rev. Lett.* **96**, 142502 (2006).
- [7] Zs. Fülöp, Á.Z. Kiss, E. Somorjai, C.E. Rolfs, H.P. Trautvetter, T. Rauscher, and H. Oberhummer, *Z. Phys. A* **355**, 203 (1996).
- [8] W. Rapp, H.J. Brede, M. Heil, D. Hentschel, F. Käppeler, H. Klein, R. Reifarh, and T. Rauscher, *Nucl. Phys.* **A688**, 427 (2001).
- [9] Gy. Gyürky, G. G. Kiss, Z. Elekes, Zs. Fülöp, E. Somorjai, A. Palumbo, J. Görres, H. Y. Lee, W. Rapp, M. Wiescher, N. Özkan, R. T. Guray, G. Efe, and T. Rauscher, *Phys. Rev. C* **74**, 025805 (2006).
- [10] N. Özkan, G. Efe, R. T. Guray, A. Palumbo, M. Wiescher, J. Görres, H. Y. Lee, Gy. Gyürky, Zs. Fülöp, and E. Somorjai, *Phys. Rev. C* **75**, 025801 (2007).
- [11] E. Somorjai, Zs. Fülöp, Á.Z. Kiss, C.E. Rolfs, H.P. Trautvetter, U. Greife, M. Junker, S. Goriely, M. Arnould, M. Rayet, T. Rauscher, and H. Oberhummer, *Astron. Astrophys.* **333**, 1112 (1998).
- [12] C. E. Laird, D. Flynn, R. L. Hershberger, and F. Gabbard, *Phys. Rev. C* **35**, 1265 (1987).
- [13] T. Sauter and F. Käppeler, *Phys. Rev. C* **55**, 3127 (1997).
- [14] J. Bork, H. Schatz, F. Käppeler, and T. Rauscher, *Phys. Rev. C* **58**, 524 (1998).
- [15] F. R. Chloupek, A. StJ. Murphy, R. N. Boyd, A. L. Cole, J. Görres, R. T. Guray, G. Raimann, J. J. Zach, T. Rauscher, J. V. Schwarzenberg, P. Tischhauser, and M. C. Wiescher, *Nucl. Phys.* **A652**, 391 (1999).
- [16] Gy. Gyürky, E. Somorjai, Zs. Fülöp, S. Harissopoulos, P. Demetriou, and T. Rauscher, *Phys. Rev. C* **64**, 065803 (2001).
- [17] S. Harissopoulos, E. Skreti, P. Tsagari, G. Souliotis, P. Demetriou, T. Paradellis, J. W. Hammer, R. Kunz, C. Angulo, S. Goriely, and T. Rauscher, *Phys. Rev. C* **64**, 055804 (2001).
- [18] N. Özkan, A. StJ. Murphy, R. N. Boyd, A. L. Cole, M. Famiano, R.T. Guray, M. Howard, L. Sahin, J.J. Zach, R. deHaan, J. Görres, M. C. Wiescher, M.S. Islam, and T. Rauscher, *Nucl. Phys.* **A710**, 469 (2002).
- [19] S. Galanopoulos, P. Demetriou, M. Kokkoris, S. Harissopoulos, R. Kunz, M. Fey, J. W. Hammer, Gy. Gyürky, Zs. Fülöp, E. Somorjai, and S. Goriely, *Phys. Rev. C* **67**, 015801 (2003).
- [20] Gy. Gyürky, Zs. Fülöp, E. Somorjai, M. Kokkoris, S. Galanopoulos, P. Demetriou, S. Harissopoulos, T. Rauscher, and S. Goriely, *Phys. Rev. C* **68**, 055803 (2003).
- [21] P. Tsagari, M. Kokkoris, E. Skreti, A. G. Karydas, S. Harissopoulos, T. Paradellis, and P. Demetriou, *Phys. Rev. C* **70**, 015802 (2004).
- [22] Gy. Gyürky, G. G. Kiss, Z. Elekes, Zs. Fülöp, E. Somorjai, and T. Rauscher, *J. Phys. G* **34**, 817 (2007).
- [23] S. Kailas, M.K. Mehta, S.K. Gupta, Y.P. Viyogi, and N.K. Ganguly, *Phys. Rev. C* **20**, 1272 (1979).
- [24] A. Mushtaq, S.M. Qaim, and G. Stöcklin, *Appl. Radiat. Isotopes* **39**, 1085 (1988).
- [25] M. R. Bhat, *Nuclear Data Sheets* **68**, 579 (1993).
- [26] B. Singh, *Nuclear Data Sheets* **74**, 63 (1995).
- [27] <http://www.nndc.bnl.gov/>
- [28] J. F. Ziegler and J. P. Biersack, code SRIM Version

- 2003.20
- [29] S. Agostinelli J. Allison, K. Amako, J. Apostolakis, H. Araujo, P. Arce, M. Asai, D. Axen, S. Banerjee, and G. Barrand, Nucl. Instr. Meth. **A506**, 250 (2003).
- [30] T. Rauscher and F.-K. Thielemann, At. Data Nucl. Data Tables **75**, 1 (2000).
- [31] T. Rauscher and F.-K. Thielemann, At. Data Nucl. Data Tables **79**, 47 (2001).
- [32] T. Rauscher and F.-K. Thielemann, in *Stellar Evolution, Stellar Explosions, and Galactic Chemical Evolution*, ed. A. Mezzacappa (IOP, Bristol 1998), p. 519.
- [33] C. Iliadis, *Nuclear Physics in Stars*, (Wiley-VCH, Berlin 2007).
- [34] P. Descouvemont and T. Rauscher, Nucl. Phys. **A777**, 137 (2006).
- [35] J. P. Jeukenne, A. Lejeune, and C. Mahaux, Phys. Rev. C **16**, 80 (1977).
- [36] A. Lejeune, Phys. Rev. C **21**, 1107 (1980).
- [37] E. Bauge, J. P. Delaroche, and M. Girod, Phys. Rev. C **58**, 1118 (1998).
- [38] E. Bauge, J. P. Delaroche, and M. Girod, Phys. Rev. C **63**, 024607 (2001).
- [39] T. Rauscher, code EXP2RATE (2003), <http://download.nucastro.org/codes/exp2rate.f>
- [40] N.A. Roughton, M.R. Fritts, R.J. Peterson, C.S. Zaidins, and C.J. Hansen, At. Data Nucl. Data Tables **23**, 177 (1979).